Available online at www.sciencedirect.com
SCIENCE DIRECT®
Journal of Sound and Vibration 270 (2004) 191–206
JOURNAL OF SOUND AND VIBRATION
www.elsevier.com/locate/jsvi

Wavelet-Galerkin method for the free vibrations of an elastic cable carrying an attached mass

M. Al-Qassab[a,*], S. Nair[b]

[a] *Department of Mechanical Engineering, University of Bahrain, P.O. Box 32038, Manama, Bahrain*
[b] *Mechanical, Materials and Aerospace Engineering Department, Illinois Institute of Technology, 10 West 32nd St., Chicago, IL 60616, USA*

Received 28 August 2002; accepted 8 January 2003

Abstract

A multilevel representation of Daubechies compactly supported wavelet has been used to study the free vibrations of elastic catenary cables carrying an attached mass. Anti-derivatives of wavelets are used to guarantee satisfaction of boundary conditions. Natural frequencies, mode shapes and dynamic tensions are obtained and compared with the classical Fourier series representation. The localization feature of wavelets has been implemented to enter the singularity region that is produced by the attached mass. More wavelets are used near the mass location and the spurious oscillations in the solution are minimized with few number of terms in the series. However, the Fourier solution shows many oscillations along the cable length and Gibbs phenomenon at the mass location. In both methods, reverting and swapping modes are discovered in which higher modes revert to lower modes and that the horizontal displacement components become greater than the vertical ones even for cables with small sag to span ratios.

1. Introduction

Because of their flexibility and light weight, cables are used in ocean engineering to carry attached masses, such as vessels, cameras, hydrophones, etc. The vibration analysis of a cable carrying an attached mass differs from that of the bare cable since the cable is no longer a smooth continuous curve. The mass is a source of singularity that disturbs the uniformity of the cable and therefore needs special attention. Sergev and Iwan [1] found the experimental and theoretical natural frequencies and mode shapes of strings with attached masses. The string was considered as a sequence of segments connected at the attached masses. The theoretical solution is found by

*Corresponding author. Tel.: +973782114; fax: +973684844.
E-mail address: malqassab@eng.uob.bh (M. Al-Qassab).

0022-460X/03/$ - see front matter © 2003 Elsevier Ltd. All rights reserved.
doi:10.1016/S0022-460X(03)00490-5

considering the wave propagation equation for each segment. They have found that the theoretical results agree with the experimental natural frequencies, node and antinode locations and the modes amplitudes. Rosenthal [2] used an iterative technique called the method of imaginary reaction to find the static configuration and Stodola's method for dynamics of slack cables with discrete masses. He studied two cases: fixed–fixed cable and fixed–free or forced cable. The effect of the added mass was included in the analysis, too. The author has provided by means of a log-log plot the modal frequencies and the cable tension for the complete range of sag to span ratio. The plot showed the phenomenon of frequency crossover and the behavior of the modes at large sag ratio. Cheng and Perkins [3] used the Hamilton's principle to derive the equations of motion of a sagged cable supporting a discrete mass. They assumed a parabolic shape for the static configuration and a linear analysis for dynamics in keeping with the linear theory presented by Irvine and Caughey [4] for bare cables. Therefore, they treated cables with small sag to span ratios only. They considered two asymptotic models. The first one neglected the tangential accelerations for both the cable and the attached mass. This model is valid for small masses only. The second model neglected only the tangential acceleration of the cable. This model is suitable for larger masses. The effect of the cable elasticity and the effect of the mass attached on the natural frequencies were shown by means of graphs. Cheng and Perkins [5] extended their work of single mass to include an array of attached masses on a cable. They obtained a closed-form solution derived from the linear theory of cable vibration. They compared their solution with the results obtained by Sergev and Iwan [1] and Rosenthal [2]. Their solution converged to the solution given by Sergev and Iwan [1] of a string supporting four equally spaced, equal masses and indistinguishable with the results of Rosenthal [2] for the example of six equal masses, unequally spaced in the range of sag to span ratio less than 1:8. The authors have shown that for a symmetric array of masses there exist symmetric and antisymmetric modes and for a large number of attached equally spaced, equal masses the solution converged to the modes of a bare cable. While for asymmetric array of masses there exist asymmetric modes only. Cheng and Perkins [6] studied the theoretical and experimental analysis of the forced response vibration of their previous work [5]. The dynamic displacements have been expressed in terms of the Green function. They used the example of four equally spaced, equal masses discussed in their previous paper for comparison. The theoretical and experimental frequency response curves have similar pattern and some discrepancies arose because of the linear assumption in the asymptotic model. Yu [7] obtained closed-form solutions of the vibration of cable under complicated loads. He solved the more general case of cable vibration under both distributed and concentrated static loading, because he added load components that act in the horizontal direction (out-of-plane direction) along with vertical loadings. Therefore the cable lay in an inclined plane and the in-plane and out-of-plane equations of motions are now coupled. He modified the transfer matrix method that was used by the previously mentioned researchers, to consider a catenary static profile. As a special case his solution reduced to the first asymptotic model discussed by Cheng and Perkins [3] for a single mass and the absence of horizontal loading.

The purpose of this paper is to study the free vibration of catenary elastic cables with mass attached using the wavelet-Galerkin method and compare with the classical Fourier method. Wavelets have proven to be an efficient tool of analysis in many fields including the solution of partial differential equations. The main feature of wavelets is that their basis functions are localized in space and the solution is represented using levels of resolution providing a hierarchy

of solution. This gives the ability to generate the matrices of a discretized problem at higher levels of resolution without regenerating the matrices throughout. Besides, there are many classes of wavelets to try such as Coiflets, Daubechies, Meyer, Morlet, splines wavelets and others. In each class there is an infinite number of wavelets. The commonly used method in solving partial differential equations is the wavelet-Galerkin method. It is important that the basis function selected must satisfy the boundary conditions and since translation is one of the main features of wavelets the boundary conditions are not satisfied. A direct way to overcome this matter is to use the anti-derivative of Daubechies wavelets as developed by Xu and Shann [8]. The anti-derivative wavelets are integral type of the wavelets that satisfy the boundary conditions. Therefore, we applied the wavelet-Galerkin method using the anti-derivative of Daubechies wavelets to guarantee the satisfaction of the boundary conditions.

2. General formulation

A suspended catenary elastic cable that carry an attached mass is shown in Fig. 1 in its equilibrium position. The kinetic energy of the system has two parts coming from the cable and from the attached mass and is given as follows:

$$K = \frac{1}{2}\int_0^l \rho(\dot{u}^2 + \dot{v}^2)\,\mathrm{d}s + \frac{1}{2}\int_0^l M\delta(s - s_o)(\dot{u}^2 + \dot{v}^2)\,\mathrm{d}s, \tag{1}$$

where dot means partial differentiation with respect to time, t and the prime means partial differentiation with respect to the space variable s, l is the cable length, ρ is the mass of the cable per unit length, M is the mass of the attached particle, s_o is the location of the attached particle, $\delta(s)$ is the Dirac delta and u and v are the cable displacement components in the horizontal and vertical directions respectively. If $\mathrm{d}S$ is the current arc length of the cable, the Lagrangian strain $\varepsilon(s,t)$ becomes

$$\varepsilon(s,t) = \frac{(\mathrm{d}S - \mathrm{d}s)}{\mathrm{d}s} = \sqrt{(x' + u')^2 + (y' + v')^2} - 1. \tag{2}$$

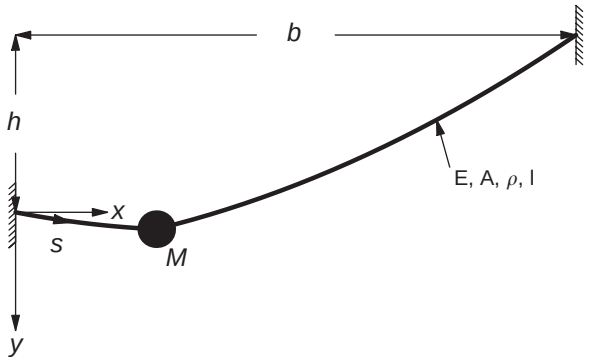

Fig. 1. Static shape of catenary cable carrying an attached mass at $s = s_o$ and the definition of the co-ordinate system.

The potential energy can be written as

$$\Pi = \int_0^l \left(T\varepsilon + \tfrac{1}{2}EA\varepsilon^2 - \rho g v - Mg\delta(s - s_o)v\right)\mathrm{d}s, \tag{3}$$

where T is the cable static tension and it is function of s, E is the modulus of elasticity and A is the cross-sectional area of the cable. Using Eqs. (1) and (3) in the Hamilton's principle

$$\delta \int_{t_1}^{t_2} (K - \Pi)\,\mathrm{d}t = 0, \tag{4}$$

and performing the variation on u and v and integrating by parts lead to

$$\int_{t_1}^{t_2}\int_0^l \Big\{(\rho + M\delta(s - s_o))\ddot{u}\delta u + (\rho + M\delta(s - s_o))\ddot{v}\delta v + \frac{(T + EA\varepsilon)}{(\varepsilon + 1)}((x' + u')\delta u' + (y' + v')\delta v') - [\rho + M\delta(s - s_o)]g\delta v\,\mathrm{d}s\Big\}\,\mathrm{d}t = 0. \tag{5}$$

The boundary conditions of a fixed cable at its two ends are given by

$$u(0, t) = v(0, t) = 0, \qquad u(l, t) = v(l, t) = 0. \tag{6}$$

3. Static configuration

A cable with an attached mass can be considered as a cable that consists of two segments connected at the location of the mass and fixed at the other ends. The equilibrium equations can be obtained from Eq. (5) by performing further integration by parts and for vanishing dynamic displacements. The governing equilibrium equations for the catenary are

$$(Tx')' = 0, \quad 0 \leqslant s \leqslant s_o \text{ and } s_o \leqslant s \leqslant l, \tag{7}$$

$$(Ty')' + \rho g = 0, \quad 0 \leqslant s \leqslant s_o \text{ and } s_o \leqslant s \leqslant l. \tag{8}$$

The interface conditions at $s = s_o$ are obtained as follows:

$$(Tx')|_{s_o^-}^{s_o^+} = 0, \tag{9}$$

$$(Ty')|_{s_o^-}^{s_o^+} = -Mg, \tag{10}$$

$$x(s_o^+) - x(s_o^-) = 0, \tag{11}$$

$$y(s_o^+) - y(s_o^-) = 0. \tag{12}$$

By referring to Fig. 1 the boundary conditions are given as follows:

$$x(0) = 0, \qquad y(0) = 0, \tag{13}$$

$$x(l) = b, \qquad y(l) = -h. \tag{14}$$

The solution of Eqs. (7) and (8) that satisfy the conditions (9)–(14) lead to a catenary shape of the cable.

4. Galerkin procedure

In the procedure of the Galerkin method, basis functions that satisfy the boundary conditions are used. Thus we assume series solutions for $u(s,t)$ and $v(s,t)$ in the form

$$u(s,t) = \sum_{m=1}^{\infty} U_m(t)\phi_m(s), \tag{15}$$

$$v(s,t) = \sum_{m=1}^{\infty} V_m(t)\phi_m(s), \tag{16}$$

where $\phi_m(s)$ is the basis function satisfying the boundary conditions given in Eq. (6). $U_m(t)$ and $V_m(t)$ are the time-dependant functions for the horizontal and vertical displacements respectively. They are the only functions that admit variations. Therefore, when substituting Eqs. (15) and (16) in Eq. (5), sets of coupled ordinary differential equations can be obtained for arbitrary functions δU_m and δV_m. In the following equations, the summation symbol has been omitted for brevity and the repeated indices indicate summation. Horizontal direction (for arbitrary δU_m):

$$\int_0^l \left\{ (\rho + M\delta(s-s_o))\phi_m\phi_n\ddot{U}_n(t) + \frac{T+EA\varepsilon}{\varepsilon+1}(x' + U_n\phi_n')\phi_m' \right\} \mathrm{d}s = 0. \tag{17}$$

Vertical direction (for arbitrary δV_m):

$$\int_0^l \left\{ (\rho + M\delta(s-s_o))\phi_m\phi_n\ddot{V}_n(t) + \frac{T+EA\varepsilon}{\varepsilon+1}(y' + V_n\phi_n')\phi_m' - (\rho + M\delta(s-s_o))g\phi_m \right\} \mathrm{d}s = 0, \tag{18}$$

where $n, m = 1, 2, \ldots, N$, N being the total number of terms in the series.

5. Fourier representation

The basis function used here is $\phi_n = \sin(n\pi s/l)$. The boundary conditions on u and v are now satisfied. In order to non-dimensionalize Eqs. (17) and (18) we define the following parameters:

$$s^* = s/l, \quad x^* = x/l, \quad y^* = y/l, \quad U_m^* = U_m/l, \quad V_m^* = V_m/l, \quad t^* = t\sqrt{T_o/\rho l^2},$$

$$T^* = T/T_o, \quad \mu = M/\rho l, \quad \alpha = EA/T_o, \quad \beta = \rho g l/EA,$$

where T_o is the horizontal component of the cable static tension. Introducing the above parameters in Eqs. (17) and (18) and retaining the linear terms only, we get a discretized system of

equations given in matrix form as follows:

$$\mathbf{M}\ddot{\boldsymbol{\gamma}} + \mathbf{K}\boldsymbol{\gamma} = \mathbf{0}, \tag{19}$$

where

$$\boldsymbol{\gamma} = \{\mathbf{U} \quad \mathbf{V}\}^{\mathrm{T}},$$

$$\mathbf{U} = [U_1^* \quad U_2^* \quad \cdots \quad U_N^*]^{\mathrm{T}}; \quad \mathbf{V} = [V_1^* \quad V_2^* \quad \cdots \quad V_N^*]^{\mathrm{T}},$$

$$\mathbf{M} = \begin{bmatrix} \mathbf{M}_1 & \mathbf{0} \\ \mathbf{0} & \mathbf{M}_1 \end{bmatrix}, \quad M_{1nm} = 1 + 2\mu \sin(m\pi s_o^*) \sin(n\pi s_o^*), \quad \mathbf{K} = \begin{bmatrix} \mathbf{K}_1 & \mathbf{K}_2 \\ \mathbf{K}_2^{\mathrm{T}} & \mathbf{K}_3 \end{bmatrix},$$

$$K_{1nm} = 2mn\pi^2 \int_0^{s_o^*} ((\alpha - T_1^*)(x_1^{*'})^2 + T_1^*) \cos(m\pi s^*) \cos(n\pi s^*)\, \mathrm{d}s^* + 2mn\pi^2 \int_{s_o^*}^1 ((\alpha - T_2^*)(x_2^{*'})^2 + T_2^*) \cos(m\pi s^*) \cos(n\pi s^*)\, \mathrm{d}s^*,$$

$$K_{2nm} = 2mn\pi^2 \int_0^{s_o^*} (\alpha - T_1^*) x_1^{*'} y_1^{*'} \cos(m\pi s^*) \cos(n\pi s^*)\, \mathrm{d}s^* + 2mn\pi^2 \int_{s_o^*}^1 (\alpha - T_2^*) x_2^{*'} y_2^{*'} \cos(m\pi s^*) \cos(n\pi s^*)\, \mathrm{d}s^*,$$

$$K_{3nm} = 2mn\pi^2 \int_0^{s_o^*} ((\alpha - T_1^*)(y_1^{*'})^2 + T_1^*) \cos(m\pi s^*) \cos(n\pi s^*)\, \mathrm{d}s^* + 2mn\pi^2 \int_{s_o^*}^1 ((\alpha - T_2^*)(y_2^{*'})^2 + T_2^*) \cos(m\pi s^*) \cos(n\pi s^*)\, \mathrm{d}s^*,$$

The subscripts 1 and 2, in x, y and T, indicate the left and right segments of the cable respectively. To find the natural frequencies, we assume harmonic motion such that $\boldsymbol{\gamma} = \mathbf{a}\sin(\bar{\omega}t^*)$, where $\mathbf{a}$ denotes the eigenvector (mode shape) and $\bar{\omega}$ represents the normalized natural frequency and it is given by $\bar{\omega} = \omega/\sqrt{\rho l^2/T_o}$, where ω is the natural frequency. Since $\mathbf{M}$ is a positive definite matrix, we can use Cholesky decomposition. The eigen system can be solved numerically using an iterative algorithm [9].

6. Wavelet representation

The basis functions we employ here are the anti-derivative wavelets that satisfy the boundary conditions of our problem. A wavelet is a localized function on the real line $\mathbb{R}$ (see, Refs. [10–12]). It occupies only an interval, say $[a, b]$, and outside this interval it is zero. This interval is determined by translation and dilation of the wavelet along the real line. If $\psi \in L^2[\mathbb{R}]$ is a wavelet then its translation and dilation is represented by

$$\psi_{jk}(x) = 2^{j/2}\psi(2^j x - k),$$

where $j,k\in\mathbb{Z}$ ($\mathbb{Z}$: the set of all integers). The anti-derivative wavelets are derived by Xu and Shann [8] to smooth out the wavelets and to easily satisfy the boundary conditions. They considered the anti-derivative of Daubechies compactly supported wavelets to represent functions in the Sobolev frames. For Dirichlet boundary conditions the anti-derivative wavelet is defined as

$$\Psi_{jk}(x)=\int_0^x \psi_{jk}\,\mathrm{d}s - x\bar{\psi}_{jk} \quad \text{for } 0\leqslant x\leqslant R, \tag{20}$$

where $\bar{\psi}_{jk}=\frac{1}{R}\int_0^R \psi_{jk}\,\mathrm{d}s$, $R=2p-1$ and p is the wavelet order. For the evaluation of the integral term in Eq. (20) we can use the algorithm given by Chen et al. [13], so that

$$\Psi_{jk}(x)=2^{-j/2}\left[\theta(2^j x-k)-\theta(-k)-\frac{x}{R}(\theta(2^j R-k)-\theta(-k))\right] \quad \text{for } 0\leqslant x\leqslant R, \tag{21}$$

where $\theta(x)=\int_0^x \psi\,\mathrm{d}s$, $j\geqslant -1$ and

$$k\in D_j \Leftrightarrow \begin{cases} 1-R\leqslant k\leqslant p-1 & \text{if } j=-1,\\ p-R\leqslant k\leqslant 2^j R-p & \text{if } j\geqslant 0. \end{cases} \tag{22}$$

An example of wavelet and anti-derivative wavelet are shown in Fig. 2. The approximate solutions of the dynamic displacements are represented by

$$u_J(s,t)=\sum_{j=-1}^{J-1}\sum_{k\in D_j} U_{jk}(t)\Psi_{jk}(s), \tag{23}$$

$$v_J(s,t)=\sum_{j=-1}^{J-1}\sum_{k\in D_j} V_{jk}(t)\Psi_{jk}(s), \tag{24}$$

which show multilevel representation of the displacement components. The total number of terms in the series is $N=(2^{J+1}R+R-p)$ for $J=0,1,2,\ldots$, etc. For convenience, some of the dimensionless parameters need to be changed. The ones that are not mentioned below are unchanged:

$$s^*=sR/l,\quad x^*=xR/l,\quad y^*=yR/l,\quad U^*_{jk}=U_{jk}R/l,\quad V^*_{jk}=V_{jk}R/l,\quad \mu^*=MR/\rho l.$$

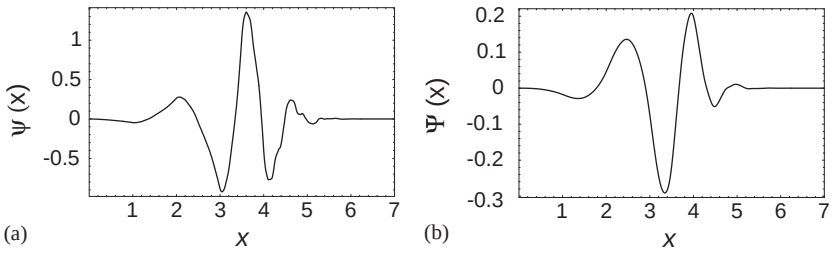

Fig. 2. (a) Wavelet and (b) anti-derivative wavelet of Daubechies wavelet of order $p=4$.

Using the basis $\phi = \Psi_{jk}(s)$ and the above dimensionless parameters we can derive the matrices of the linear system as follows:

$$\mathbf{M}\ddot{\boldsymbol{\gamma}} + \mathbf{K}\boldsymbol{\gamma} = \mathbf{0}, \tag{25}$$

where $\boldsymbol{\gamma}$ is as before and

$$\mathbf{M} = \begin{bmatrix} \bar{\mathbf{M}} & \mathbf{0} \\ \mathbf{0} & \bar{\mathbf{M}} \end{bmatrix}, \quad \bar{\mathbf{M}}_{\varsigma\eta} = \int_0^R \Psi_\varsigma \Psi_\eta \, \mathrm{d}s^* + \mu^* \Psi_\varsigma(s_o^*)\Psi_\eta(s_o^*)$$

$$\mathbf{K} = \begin{bmatrix} \mathbf{K}_1 & \mathbf{K}_2 \\ \mathbf{K}_2^{\mathrm{T}} & \mathbf{K}_3 \end{bmatrix},$$

$$K_{1\varsigma\eta} = R^2 \int_0^{s_o^*} ((\alpha - T_1^*)(x_1^{*'})^2 + T_1^*)\Psi'_\varsigma(s^*)\Psi'_\eta(s^*)\,\mathrm{d}s^* + R^2 \int_{s_o^*}^R ((\alpha - T_2^*)(x_2^{*'})^2 + T_2^*)\Psi'_\varsigma(s^*)\Psi'_\eta(s^*)\,\mathrm{d}s^*,$$

$$K_{2\varsigma\eta} = R^2 \int_0^{s_o^*} (\alpha - T_1^*)x_1^{*'}y_1^{*'}\Psi'_\varsigma(s^*)\Psi'_\eta(s^*)\,\mathrm{d}s^* + R^2 \int_{s_o^*}^R (\alpha - T_2^*)x_2^{*'}y_2^{*'}\Psi'_\varsigma(s^*)\Psi'_\eta(s^*)\,\mathrm{d}s^*,$$

$$K_{3\varsigma\eta} = R^2 \int_0^{s_o^*} ((\alpha - T_1^*)(y_1^{*'})^2 + T_1^*)\Psi'_\varsigma(s^*)\Psi'_\eta(s^*)\,\mathrm{d}s^* + R^2 \int_{s_o^*}^R ((\alpha - T_2^*)(y_2^{*'})^2 + T_2^*)\Psi'_\varsigma(s^*)\Psi'_\eta(s^*)\,\mathrm{d}s^*,$$

where ς and η have been used to denote the double indices $\varsigma = (i,j)$ and $\eta = (m,n)$. Since $\mathbf{M}$ is a positive definite matrix, we can use Cholesky decomposition and follow the same procedure of the previous section to solve for the eigensystem.

7. Results and discussions

We considered a cable of length $l = 2002.37$ m that has level supports, $h = 0$, a span $b = 2000$ m and elastic parameter $\beta = \rho g l/EA = 1/5000$. A centrally attached mass was considered with a mass ratio of $\mu = 0.1$. The parameter α then becomes $\alpha = 732$. The wavelet function used is the Daubechies wavelet of the fourth order, $p = 4$. Table 1 shows the first six natural frequencies of the cable obtained by Fourier and wavelet methods using $N = 59$. The two methods are identical to five significant figures as shown. The mode shapes of the horizontal and vertical displacement components of selected modes are shown in Fig. 3 as obtained by Fourier solution. The wavelet solution is identical to the Fourier solution. The mode shapes are normalized with respect to the vertical displacement component so that its maximum value is always made equal to

Table 1
Selected frequencies obtained by using Fourier and wavelet solutions

Mode no.	Fourier	Wavelet
1	4.6548	4.6548
2	6.2777	6.2777
3	8.7329	8.7329
4	12.573	12.573
5	14.515	14.515
6	18.862	18.862

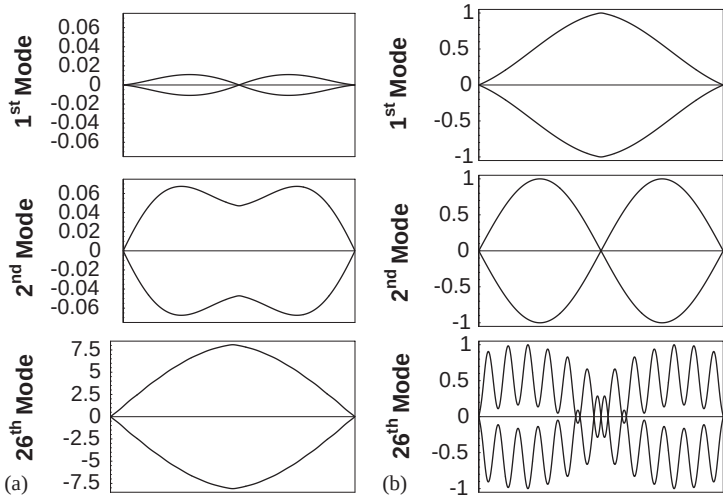

Fig. 3. Normalized mode shapes of selected modes: (a) horizontal displacements and (b) vertical displacements.

one. The first and second modes are similar to the first and second modes of the same cable if $\mu = 0$. The first two and the subsequent mode shapes will continue to behave similarly to those of the bare cable except that for the attached mass problem the vertical displacement components of the symmetric modes will have cusps at the mass location. Similarly, the horizontal displacement components will have cusps at the mass location but in the antisymmetric modes. The cusps become sharper as the mass ratio is increased. Mode 26 is similar to mode 30 of the bare cable which is the first reverting partially swapping mode first reported by AL-Qassab and Nair [14]. In this mode the horizontal displacement component is larger than the vertical displacement component. The reverting partially swapping modes appear in our solutions because we have not neglected the horizontal inertia in the analysis. Researchers who used order of magnitude analysis in which the horizontal displacement was always assumed smaller than the vertical displacement failed to discover the reverting modes. Those who used numerical techniques considered the first few lower modes and missed the opportunity to find the reverting modes. As an illustration, a comparison is made with the method explained by Cheng and Perkins [3] as shown in Table 2. The numbering of modes is based on the present method. Since they based their analysis on the linear

Table 2
Comparison of frequencies calculated by Cheng and Perkins and the present method

Mode no.	Cheng and Perkins [3]	Present method (Fourier)
1	4.658	4.6548
2	6.2818	6.2777
⋮		
25	75.9136	76.4443
26	—	77.4206
27	81.6813	81.7578

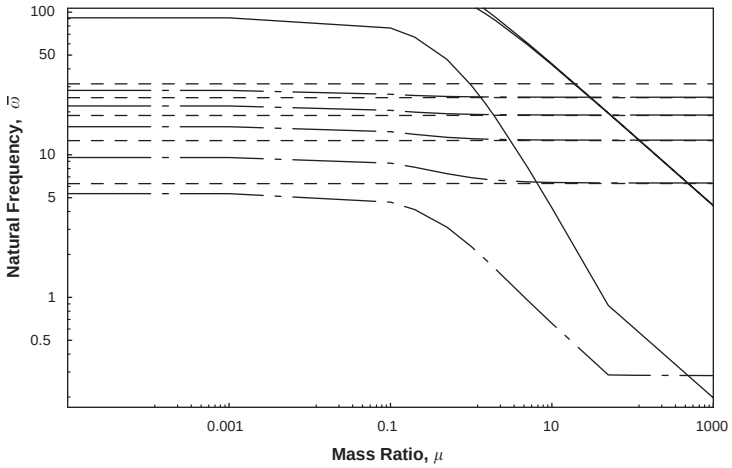

Fig. 4. Effect of the mass ratio on the natural frequencies. - - - - -; antisymmetric modes, ——– – ——–; symmetric modes, ————; reverting modes.

theory which has been developed by Irvine and Caughey [4] they failed to produce the reverting modes in their solution. Therefore, mode 27 is actually mode 26 in their solution.

The effect of increasing the mass ratio on the modes is shown in Fig. 4. It is interesting to notice that the reverting modes are moving towards the lower modes and creating what is known as frequency crossover. For very large mass ratios the first mode of oscillation is of a reverting mode type.

Fig. 5 shows the dynamic tension of the cable associated with the fundamental mode of vibration as obtained by Fourier and wavelet methods for different number of terms, N. We notice that both methods show the peak of oscillation at the mass location. However, the Fourier solution shows more oscillation along the cable length too, whereas the wavelet solution shows smooth line except at the mass location. Those oscillations are in the form of wavelets with their width getting narrower as N is increased and eventually the oscillations will diminish as N becomes large. Fig. 6 shows a log plot of the absolute values of the series coefficients versus the number of terms for the horizontal and vertical displacements of the fundamental mode using $N = 227$. Both Fourier and wavelet series coefficients are shown in a manner similar to the frequency spectrum. The coefficients are normalized by dividing by the maximum coefficient of

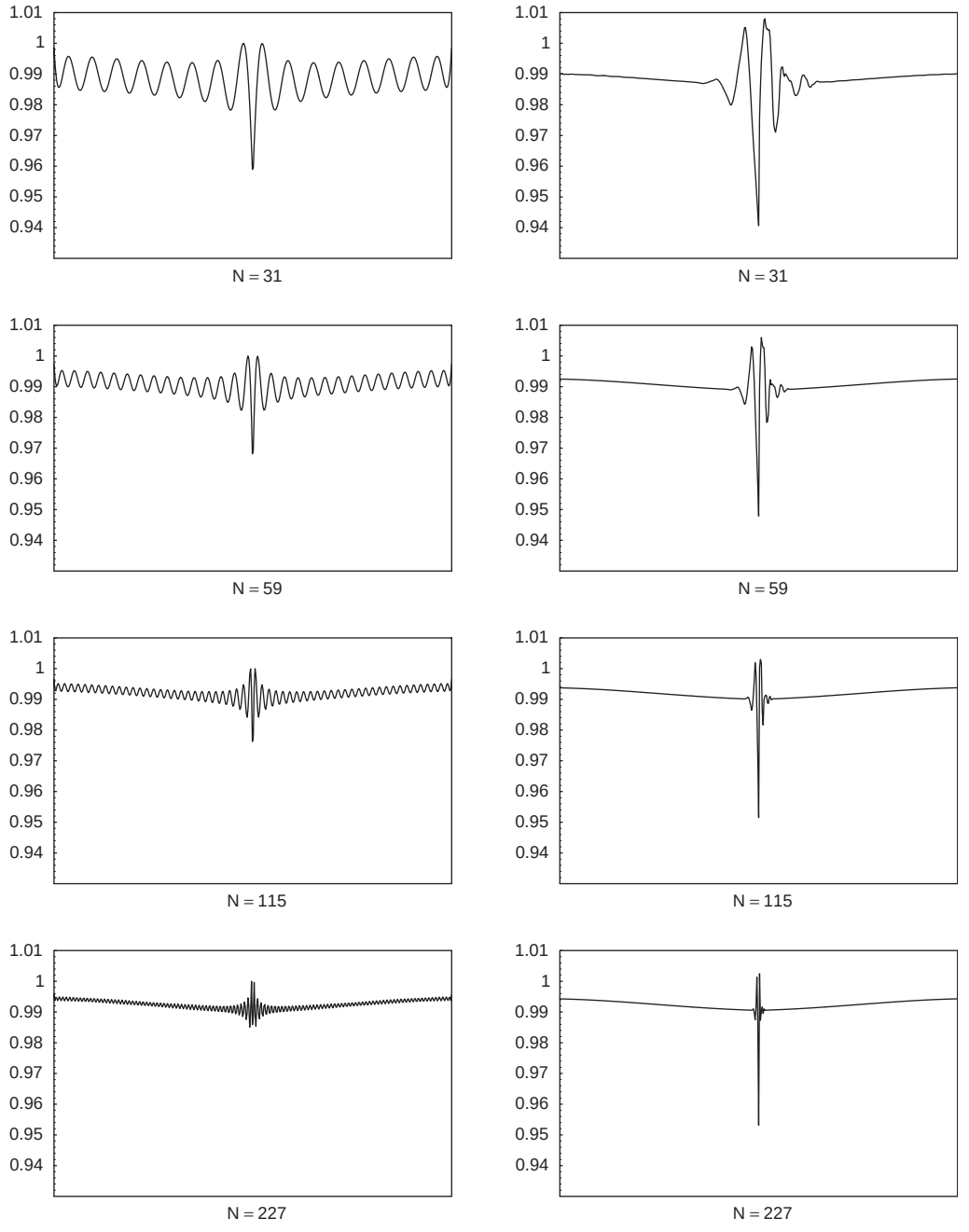

Fig. 5. First mode dynamic tension of the cable with a centrally attached mass as obtained by Fourier method (left) and wavelet method (right): $\mu = 0.1$.

the vertical displacement. The Fourier solution shows that the coefficient amplitudes are decreasing as N is increasing. The wavelet coefficients are also decreasing with increasing N except at the mass location. For levels 2–4 the coefficients of the wavelets that overlap the mass location

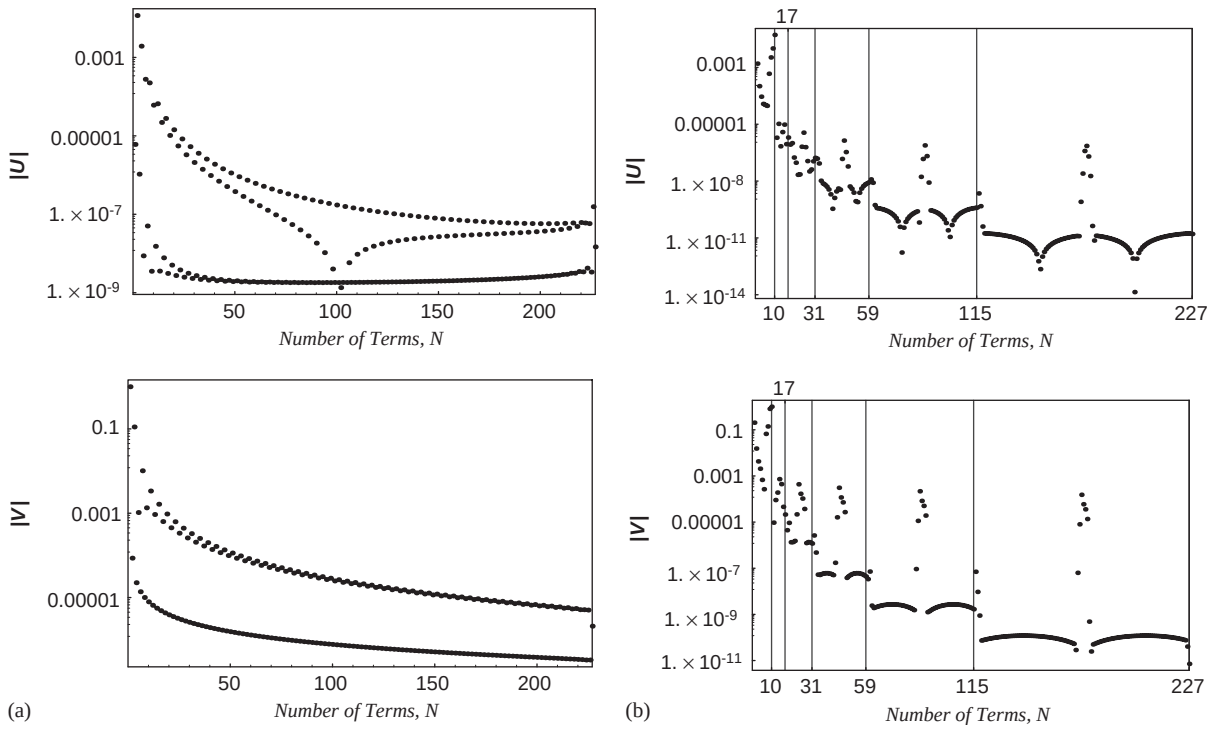

Fig. 6. Coefficient amplitudes versus the number of terms. (a) Fourier coefficients and (b) wavelet coefficients.

are very large and are as significant as those found in level 1. Moreover, they are a factor of millions greater than the rest of the coefficients. Therefore, as can be seen from the figure, there are about five terms which make strong contribution to the solution in the resolution levels following $J = 1$ and the rest can be ignored without affecting the solution. Hence, if we found that the solution is satisfactory with level J everywhere along the cable length except at the mass location we add only those five terms in the subsequent levels greater than J. The terms that should be added for a particular level $j > J$ are given by the following equation:

$$2^j s_o^* - (R-2) \leqslant k \leqslant 2^j s_o^* - 1, \quad J < j \leqslant J_{max}, \tag{26}$$

where k is the number of term added so that the corresponding wavelet has interaction with the singular point and J_{max} is the maximum level used. Fig. 7 shows the effect of the above procedure on the dynamic tension of mode 1. It is clear that the solution using $J = 1$ and $J_{max} = 4$ with $N = 46$ corresponds to the one with $N = 227$ shown in Fig. 5. Unfortunately, the singularity cannot be eliminated completely when increasing J_{max}. However, it is confined in the interval

$$s_o^* - 2^{-J_{max}} \leqslant s^* \leqslant s_o^* + 2^{-J_{max}}. \tag{27}$$

A slack cable with heavy mass located at quarter length of the cable is now considered. The same cable of the previous example is used with the following changes; span $b = 1500$ m, mass ratio $\mu = 5$, $s_o^* = 0.25$ and $\alpha = 4598$. The other parameters are kept the same. The segment of the cable between the left support and the location of the mass is taut while the second segment is

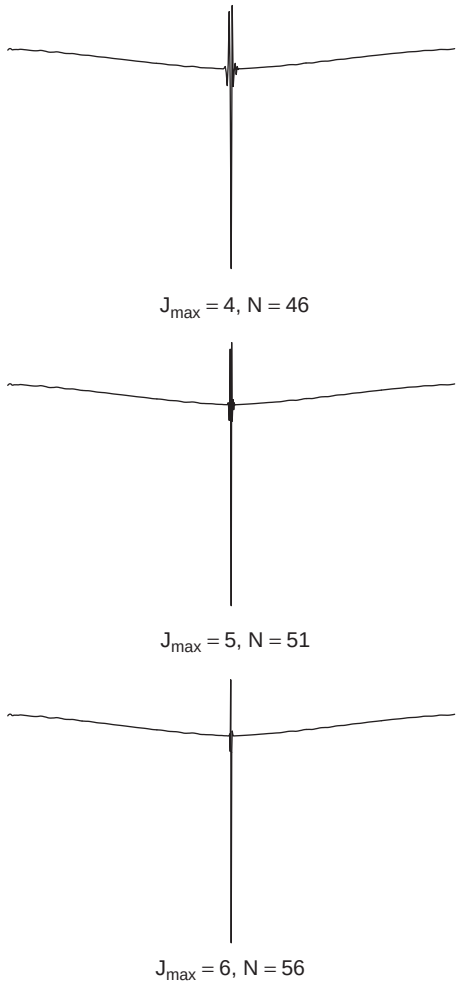

Fig. 7. Dynamic tension of mode one using $J = 1$ and allowing J_{max} to vary.

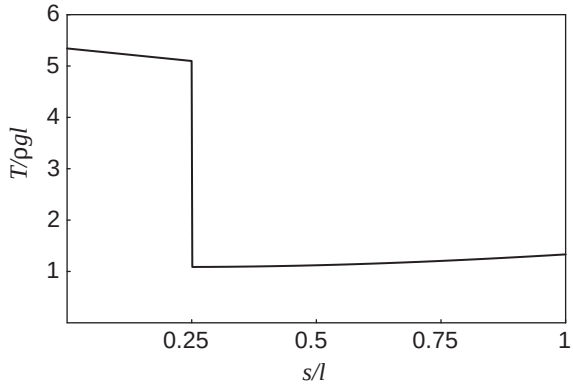

Fig. 8. Normalized static tension of the cable: $\mu = 5$; $s_o^* = 0.25$.

Table 3
Comparison of frequencies as obtained by Fourier and wavelet methods

Mode no.	Fourier, $\bar{\omega}_F$	Wavelet, $\bar{\omega}_W$	$\frac{\bar{\omega}_F-\bar{\omega}_W}{\bar{\omega}_F}100$
1	2.9618	2.9340	0.94
2	8.5902	8.5151	0.87
3	12.6844	12.5768	0.85
4	17.4575	17.3094	0.85
5	21.6318	21.4499	0.84
6	26.2609	26.039	0.84
7	28.1852	27.7568	1.52

slack as can be seen in Fig. 8, in which the tension in the left segment is about five times greater than the tension in the right segment. Fig. 8 also shows the sudden drop in the tension at the location of the mass. For the wavelet solution, all the terms in the levels up to $J = 3$ will be considered and only five terms in the subsequent levels up to $J_{max} = 6$ will be added. Thus, the total number of terms becomes, $N = 130$. Same number of terms in the Fourier solution will be used for the sake of comparison. In Table 3 the natural frequencies as obtained by Fourier and wavelets methods are compared. The percentage of errors of mode 1–6 are less than 1%, while for mode 7 it is approximately 1.5%. The differences between the two methods are more noticeable than those found in Table 1 of the previous example. Fig. 9 shows the normalized dynamic displacements and dynamic tensions for modes 1, 2, 7 and 14 as obtained by Fourier and wavelet methods. The node locations found in the Fourier solution are ahead of those found in the wavelet solution. In modes 1, 2 and similar modes the vertical displacement components are greater than the associated horizontal displacement components with maximum peaks occurring to the right of the attached mass and almost negligible displacements to the left of the attached mass. This is mainly true in the vertical components. Moreover, the vertical components of the right segment behave similarly to those of a horizontally supported bare cable. The maximum peaks in the horizontal components are always found to be the first peak from the right support. In modes 7 and 14 and similar modes, the horizontal displacement components are greater than the vertical ones, with the left segments of horizontal components reverting to the right segments of the vertical components of modes 1, 2 and similar modes respectively. Mode 14 shows large differences between the wavelet and Fourier solutions in which the maximum peak in the vertical component in the Fourier solution is found in the right segment, whereas it is found in the left segment in the wavelet solution. The horizontal components associated with mode 14 are almost identical in both methods but due to the normalization they look different in scale.

The dynamic tensions in all the modes exhibit sudden drop at the mass location. The Fourier solution shows many spurious oscillations along the cable length and Gibbs phenomenon at the mass location. Whereas, in the wavelet solution the oscillations are eliminated along the cable length and confined at the mass location in a small region given by Eq. (27), it is noticed, in the dynamic tensions as obtained by Fourier solution, that in modes 1, 2 and similar modes there are more oscillations in the left segment and in modes 7, 14 and similar modes there are more oscillations in the right segment. In any case, this gives the indication of presence of error in the Fourier solution.

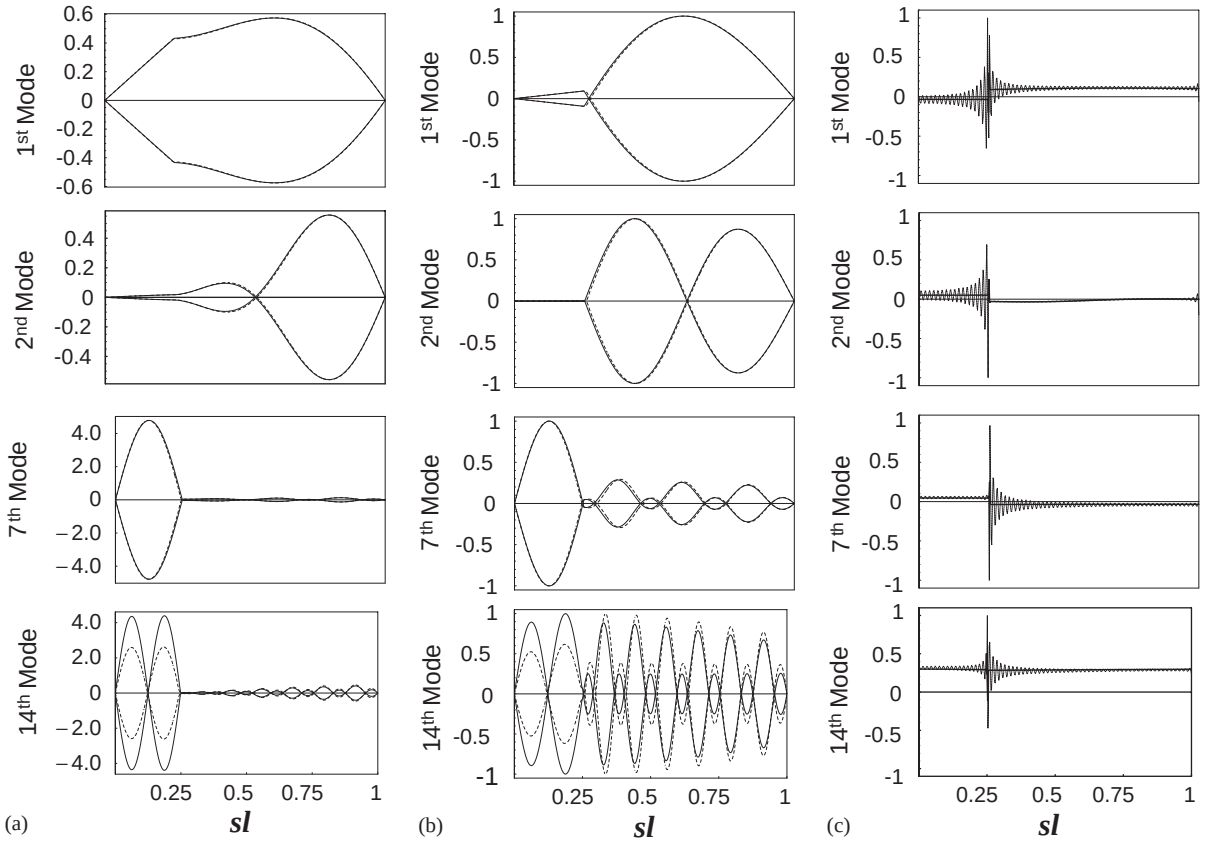

Fig. 9. Normalized (a) horizontal displacements, (b) vertical displacements and (c) dynamic tensions. ————; wavelet solution, - - - - - ; Fourier solution.

8. Conclusion

The free vibration of a catenary cable carrying an attached mass was formulated using the Hamilton's principle. The equations of motion are linearized and a Galerkin solution was applied with Fourier and wavelet representations. Comparisons between Fourier and wavelet solutions are presented that include the cable natural frequencies, the mode shapes and the dynamic tensions of the cable at different mode numbers and using different number of terms, N, for both methods.

As far as the natural frequencies and mode shapes are concerned the Fourier and wavelet solutions are generally in good agreement. As far as the dynamic tension is concerned the Gibbs phenomenon is clearly shown to exist at the mass location in the Fourier solution. Whereas, the oscillations in the wavelet solution are found only at the mass location. The singularity region is made very small by considering only the wavelets that interact with it and hence achieving better results with fewer terms. Because of the inclusion of the inertia term of the horizontal displacement component in the analysis, reverting modes are found. For such modes the

horizontal displacement components are greater than the associated vertical displacement components. The reverting modes might be higher modes in bare cables but they move towards the lower modes as the mass ratio is increased.

References

[1] S.S. Sergev, W.D. Iwan, The natural frequencies and mode shapes of cables with attached masses, *Journal of Energy Resources Technology* 103 (1981) 237–242.
[2] F. Rosenthal, Vibrations of slack cables with discrete masses, *Journal of Sound and Vibration* 78 (4) (1981) 573–583.
[3] S.P. Cheng, N.C. Perkins, Free vibration of a sagged cable supporting a discrete mass, *Journal of the Acoustical Society of America* 91 (5) (1992) 2654–2662.
[4] H.M. Irvine, T.K. Caughey, The linear theory of free vibrations of a suspended cable, *Proceedings of the Royal Society, London* A-341 (1974) 299–315.
[5] S.-P. Cheng, N.C. Perkins, Closed-form vibration analysis of sagged cable/mass suspensions, *Journal of Applied Mechanics* 59 (1992) 923–928.
[6] S.-P. Cheng, N.C. Perkins, Theoretical and experimental analysis of the forced response of sagged cable/mass suspensions, *Journal of Applied Mechanics* 61 (1994) 944–948.
[7] P. Yu, Explicit vibration solutions of a cable under complicated loads, *Journal of Applied Mechanics* 64 (1997) 957–964.
[8] J.-C. Xu, W.-C. Shann, Galerkin-wavelets method for two-point boundary value problems, *Numerische Mathematik* 63 (1992) 123–144.
[9] *Mathematica*, Wolfram Research, Inc., Champaign, IL, 1996.
[10] I. Daubechies, Orthonormal bases of compactly supported wavelets, *Communications on Pure and Applied Mathematics* 41 (1988) 909–996.
[11] I. Daubechies, *Ten Lectures on Wavelets*, CBMS-NSF Regional Conference Series, in Applied Mathematics, SIAM, Philadelphia, PA, 1992.
[12] E. Hernandez, G. Weiss, *A First Course on Wavelets*, CRC Press, Boca Raton, FL, 1996.
[13] M.-Q. Chen, C. Hwang, Y.-P. Shih, The computation of wavelet-Galerkin approximation on a bounded interval, *International Journal for Numerical Methods in Engineering* 39 (1996) 2921–2944.
[14] M. AL-Qassab, S. Nair, Wavelet-Galerkin method for the free vibrations of an elastic cable, *Journal of Engineering Mechanics, American Society of Civil Engineers* 129 (3) (2003) 350–357.